# Spatial-frequency tuning of visual contour integration

**S. C. Dakin and R. F. Hess**

*Department of Ophthalmology, McGill Vision Research, 687 Pine Avenue West H4-14, Montreal, Quebec, Canada H3A 1A1*

Received October 14, 1997; revised manuscript received January 29, 1998; accepted January 30, 1998

We examine the mechanism that subserves visual contour detection and particularly its tuning for the spatial frequency of contour components. We measured the detection of contours composed of Gabor micropatterns within a field of randomly oriented distractor elements. Distractors were randomly assigned one of two spatial frequencies, and elements lying along the contour alternated between these values. We report that the degree of tolerable spatial-frequency difference between successive contour elements is inversely proportional to the orientation difference between them. Spatial-frequency tuning (half-width at half-height) for straight contours is ~1.3 octaves but, for contours with a 30° difference between successive elements, drops to ~0.7 octaves. Integration of curved contours operates at a narrower bandwidth. Much orientation information in natural images arises from edges, and we propose that this narrowing of tuning is related to the reduction in interscale support that accompanies increasing edge curvature. © 1998 Optical Society of America [S0740-3232(98)01006-0]

*OCIS codes:* 330.7310, 330.5510, 330.4060, 330.4270, 330.6110.

## 1. INTRODUCTION

The development of effective psychophysical measures of contour detectability has led to a resurgence of interest in the principles underlying visual grouping as first espoused by the Gestaltists. Field *et al.*[1] measured the detectability of targets composed of Gabor patches whose orientations and positions were consistent with the presence of a smooth contour. These "paths" were embedded in a field of randomly oriented Gabor patches. Subjects' ability to detect paths depends primarily on the relative orientation of elements lying along the path (the path angle) and not on factors such as inter-element spacing. In short, straight or near-straight paths are much easier to detect than convoluted paths. The importance of local orientation in determining perceived contour structure has been confirmed with closed contours[2,3] and with other texture patterns, such as dotted lines in noise[4,5] and Glass patterns.[6–8]

These data are generally consistent with the presence of a mechanism that integrates sets of local orientation estimates into coherent visual contours. Given the wealth of evidence suggesting that the primary visual cortex performs a local image decomposition along the dimensions of spatial frequency and orientation, V1 cells are natural candidates for the local orientation estimators. That paths can be integrated across depth[9] strengthens the proposition that the site of integration is cortical. A number of computational integration schemes that share broadly similar preprocessing (a cortical filter bank) have been implemented to combine local orientation estimates into contours. Zucker and co-workers[10–13] propose that an initial estimate of the local orientation field is refined with an iterative, relaxation-labeling algorithm to maximize a measurement of local co-circularity. Sha'shua and Ullman[14] describe a saliency map that weights in proportion to contour length and in inverse proportion to contour curvature. Yen and Finkel[15,16] use a linear quadrature steerable filter pyramid[17] followed by interaction by means of horizontal connections that encode co-circularity constraints.[12] Connections include one set of fan-out excitatory connections for orientations consistent with a contour and one set extending orthogonal to the cells' preferred direction. In the final stage of this scheme contours are perceptually bound by means of synchronization of cells firing.

Such models raise issues of computational complexity and the appropriateness of using iterative maximization to achieve consistency of local orientation signals. Furthermore, the issue of how linking processes in such systems corrupt a neuronal code for contrast remains controversial. There is evidence for facilitation of contrast detection for elements within contours,[18] but there is no effect of contour inclusion on perceived contrast nor any effect of contrast variation (within the visible range) on contour detection.[19] The alternative to interactive systems is a feed-forward approach. Gigus and Malik[20] describe a system that adaptively tunes local filters to near-circular image structure. One of us[8] demonstrated that selection of the output of the most locally active filter, across filter orientation, gives contour integration that is sufficient to explain psychophysical performance at detecting contourlike structure in Glass patterns. The latter approaches both have the advantage of being nonitterative and therefore of lending themselves to parallel implementation.

However, all of the work described treats only one class of regularity arising from to the presence of contours in images: correlations in orientation across space and within a single spatial-frequency band. Field *et al.*,[1] for example, state, "We believe that with many natural edges

 

it may be useful to solve the continuity problem separately at each scale" (p. 174). This approach avoids difficult (and more general) questions of how information is combined from mechanisms tuned to multiple spatial frequencies. However, real contours are supported not only by correlated activity across space but also from the activity of filters at the same location across scale. Natural images produce higher correlations in the output of filters located at similar positions and in adjacent frequency bands than do noise images with identical $(1/f^2)$ power spectra.[21] Such interscale correlations are attributable directly to the phase structure of edges, which phase-randomized images lack. Indeed many edge-detection schemes[22–25] exploit this regularity. Marr[23] specifies this constraint in the form of his spatial-coincidence assumption: "If a zero-crossing is present in a set of independent LoG channels over a contiguous range of sizes, and the segment has the same position and orientation in each channel, then the set of such zero-crossing segments indicates the presence of an intensity change in the image that is due to a single physical phenomenon" (p. 70). It has been proposed that the visual system tracks such local phase alignments (over possibly much smaller spatial-frequency intervals) to determine the correct spatial scale of analysis.[26] Inappropriate application of phase tracking to determine spatial scale can explain Harmon and Julesz's[27] so-called critical masking phenomena for blocked face images.[26,28] Similarly, sensitivity to phase tracks has been demonstrated for motion-discrimination tasks by use of blocked fractal images.[29]

Figure 1 illustrates two variants on an association-field model,[1] which address the issue of scale combination. The first exploits phase alignments arising in edges by simply allowing the contour-integration mechanism to be less selective in the spatial frequency of elements that it integrates. The advantage of such a system is that it will be resistant to scale variation along contours, but the price paid is vulnerability to the intrusion of noise. A second approach is depicted in Fig. 1(b), where contours are extracted within an individual spatial scale (as assumed with the models described above), and then interscale support is sought for the presence of a contour. The problem with this approach is that it poses a correspondence problem for contours between scales that may be compounded by contour incompleteness.

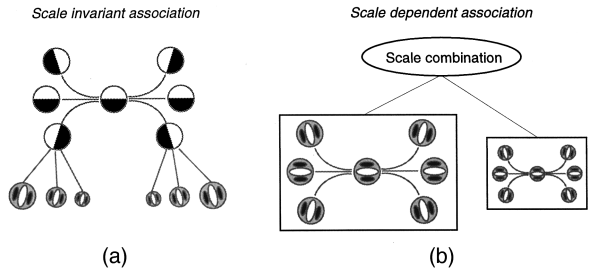


Fig. 1. Two variants on the association field model that deal with variation in spatial scale of contour elements. (a) The scale-invariant model performs contour integration on orientation tokens that are abstracted from filter outputs across scale. (b) The scale-dependent model has association operations at multiple, independent spatial scales, and combination occurs after integration.

Note that the second model represents only one of many possible approaches to scale combination. Because the purpose of the experiments reported here is to measure spatial-frequency tuning and not to localize the site of scale combination, we are not considering, for example, the possibility that scale combination occurs before contour extraction. Psychophysical results are assessed in the context of these models, but the model in Fig. 1(b) should be considered only as an exemplar of one of many possible schemes for combining multiscale image structure.

To summarize, it appears that there is a gap between what is known of the structure of contours in natural images and what is encoded by computational models of visual contour extraction. Present models do not exploit across-scale correlations in the response of filters to contours. In this paper by examining how observers' detection of contours in noise is affected by fluctuations in the local spatial frequency within a contour, we ask if observers are able to exploit such correlations. To preempt our findings, we show that spatial tuning of contour extraction narrows with increasing contour curvature, thus suggesting a prominent role for interscale support for edges in the association process.

## 2. GENERAL METHODS

### A. Subjects

The authors served as subjects in the experiments reported. Both are corrected-to-normal myopes, and SCD has a small (<0.25 D) corrected astigmatism. Sufficient training was undertaken before threshold measurement for subjects to achieve asymptotic performance. Both authors are highly practiced at contour-detection tasks.

### B. Apparatus

The stimuli were generated and presented by a Macintosh 7500 microcomputer that also recorded subjects' responses. A Nanao Flexscan 6500 monochrome monitor with a frame-refresh rate of 75 Hz was used to display all stimuli. Routines from Denis Pelli's VideoToolbox[30] were the basis of the code used to display images and were also used to generate a look-up table to linearize luminance levels. The screen was viewed binocularly at a distance of 97 cm and had a mean background luminance of 23.6 cd $m^{-2}$.

### C. Stimuli: Micropatterns

Stimuli were composed of patches with luminance modulated by sinusoidal gratings that were multiplied by an isotropic Gaussian envelope (Gabor patches). This function has the form

$$G(x, y) = A \sin\left(\frac{x_t}{\lambda} + \phi\right)\exp\left(-\frac{x^2 + y^2}{2\sigma^2}\right), \qquad (1)$$

where $A$ is the amplitude of the function, $\sigma$ is the standard deviation of the Gaussian envelope, and $\lambda$ and $\phi$ are the wavelength and the phase, respectively, of the modulating sinusoid. All stimuli employed patches with $\phi$ set to 0° so that all patches were balanced for luminance (i.e.,

were in sine phase). Here $x_t$ is the $x$ coordinate rotated by angle $\theta$ from the standard rotation equations:

$$x_t = x \cos \theta + y \sin \theta,$$

$$y_t = y \cos \theta - x \sin \theta. \quad (2)$$

Patches were spatially truncated at $\pm 2.5\sigma$ and had their contrast fixed at 90%. The Gaussian space constant of the Gabor envelope was fixed at 9.4 arc min (8 pixels). The wavelength of the modulating sinusoid was varied across conditions and ranged from 32 to 4 pixels [1.6–12.8 cycles per degree (c.p.d.)]. Note that changing the wavelength of the carrier with a fixed Gaussian window changes the spatial bandwidth as well as the spatial frequency of the micropattern. To measure pure spatial-frequency differences involves the use of locally scaled versions of patches that in turn alters the sparseness of stimuli. We chose to fix all stimulus parameters except carrier wavelength but consider the possible effect of bandwidth variation in a control condition reported at the end of experiment 2.

### D. Stimuli: Contour Generation

Cued stimuli were composed of a path embedded in a background of distractors. The procedure for path construction is described in detail elsewhere.[1] Briefly, the path had a backbone of 8 invisible line segments of length 67 pixels and joined at an angle uniformly distributed from $\alpha - 4°$ to $\alpha + 4°$. Here $\alpha$ is called the path angle. Gabor elements were placed at the middle of each line segment and assigned the orientation of the line segment on which it was placed. The orientation of each line segment was ambiguous (within the range 0°–360°), but traversing the path from one end to the other imposes a direction (and hence an unambiguous orientation) on each of the component line segments. Finally, the path was checked to ensure that it neither intersected itself nor looped back on itself. If it did either, the path was regenerated.

The path was inserted into the display at a random location, thus ensuring that the centers of Gabor elements occupied different cells. Empty cells were filled with randomly oriented Gabor elements. The average length of each backbone line segment (67 pixels; 1.3°) was the same as the average distance between neighboring Gabor elements in the background. Consequently, neither the local nor the global element density served as a cue to path detection from no-path stimuli. As an extra precaution against such cues, however, uncued stimuli were gener-

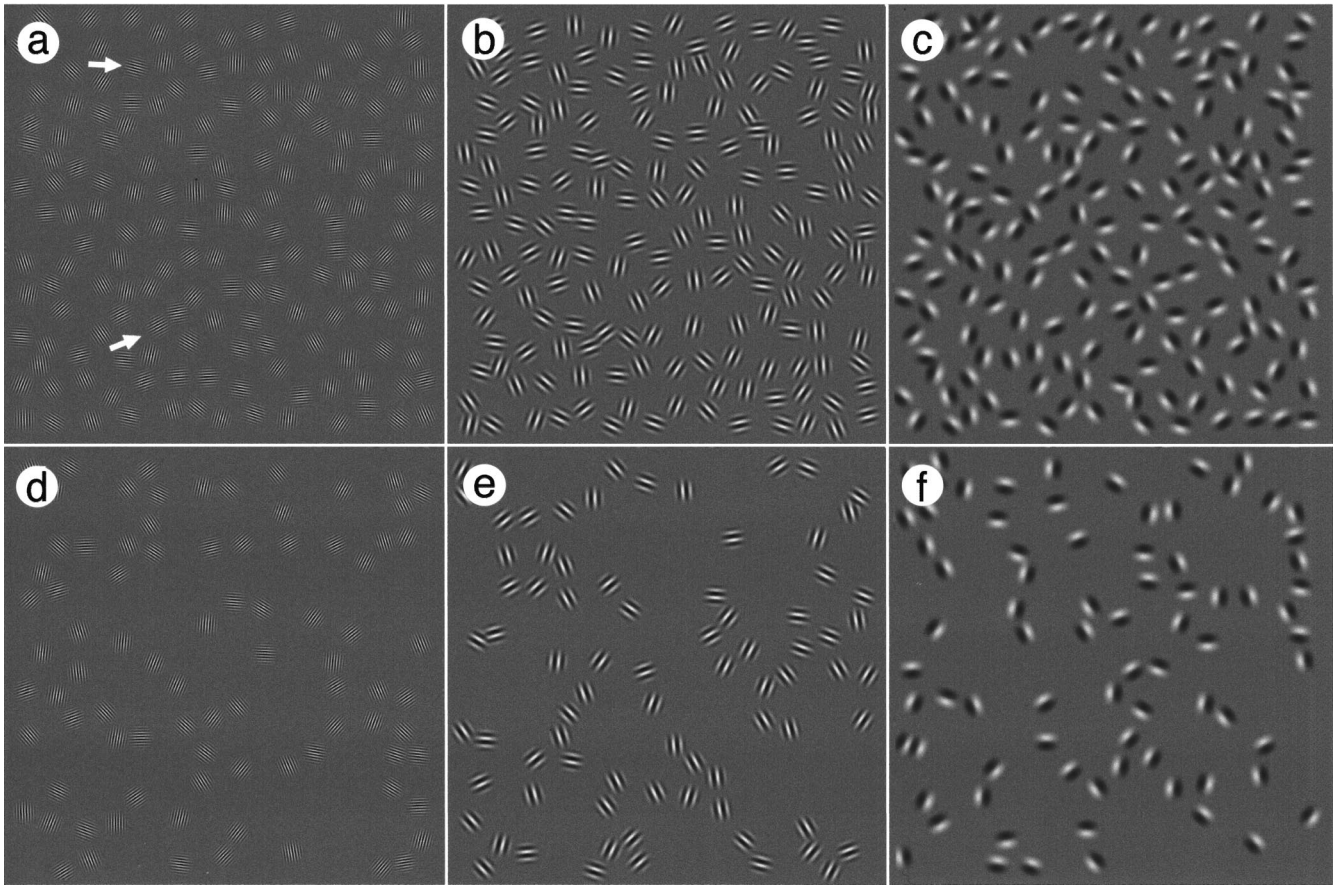


Fig. 2. Examples of the stimuli used in experiment 1. The upper row shows 8 element-long paths with a 20° difference in orientation between successive elements. Elements have spatial frequencies of (a) 12.8, (b) 4.53, and (c) 1.6 c.p.d. Paths are difficult to locate in (a) because the effective separation of micropatterns, expressed in units of carrier wavelength, is very large. The first and last elements of the path in (a) are indicated (direction of arrows indicates local contour direction). The lower row shows the similar stimuli with alternate elements along the path and half of the background elements randomly deleted. No paths are visible.

ated in the same way except that a path composed of randomly oriented elements was inserted into the background. These paths are undetectable by subjects.[9,31]

### E. Procedure

In each experiment a two-alternative-forced choice procedure was used. Subjects were presented with an image (for 500 ms), followed by a 1.0-s delay, followed by a second image (for 500 ms). One randomly selected interval had a structured path embedded in the background of distractors; the other did not. Subjects were asked to judge in which interval the path occurred.

## 3. EXPERIMENT 1: EFFECT OF OVERALL SPATIAL FREQUENCY ON CONTOUR DETECTION

### A. Method

This experiment had two parts. The first part examined whether contour extraction is affected by the spatial frequency of the patches that compose a contour. It is known that viewing distance has little effect on path detection; performance is basically insensitive to any overall scaling of the stimulus.[32] We wished to examine the effect of changing carrier spatial frequency with all other stimulus parameters equal. Figure 2 shows examples of the stimuli used in this experiment. The second part of the experiment was a control condition for subsequent experiments. From experiment 2 onward we employ stimuli composed of two populations of micropatterns differing in spatial frequency. Elements along the path alternate in spatial frequency, and we wanted to ensure that, for the stimulus parameters used (element spacing, exposure duration, etc.), the path would not be detectable if the subject simply ignored one population of Gabors. To this end we measured performance when only one population was presented to the subject (Fig. 2). Stimuli were generated in the same way as for the first part of the experiment, but the contrast of half of the elements was set to zero. For elements in the background, element contrast was randomly set to zero with a probability of 0.5; but within the path, alternate elements were "switched off."

### B. Results

Figure 3 illustrates that there is a dropoff of contour-detection performance for the highest-frequency elements (12.8 and 9.1 c.p.d.). Subjectively, this is not attributable to the visibility of Gabor micropatterns and is also unlikely to be an effect of eccentricity: Increasing exposure times (up to 5 s) to allow scanning eye movements does not significantly improve performance on the high-frequency patterns. Instead, by fixing interelement spacing the effective spacing of the high-frequency elements, expressed in units of $\lambda$ (the wavelength of the patch carrier), increases with spatial frequency. This is in agreement with Kovacs and Julesz,[2] whose use of $\lambda$ as the unit of element separation implicitly suggests that it is the critical variable for determining contour detectability (rather than the standard deviation of the Gaussian window of the patches, for example). However, to suggest that there is no role for the envelope in determining effective spacing is an oversimplification; interactions certainly arise.

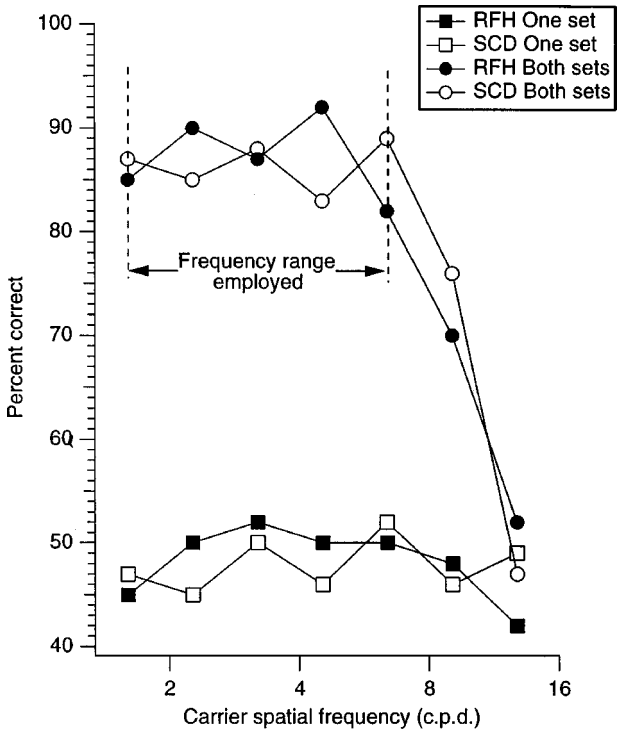


Fig. 3. Results from experiment 1. Circles show the contour detection performance of two subjects as a function of micropattern carrier spatial frequency. Paths were composed of eight elements and had a path angle of 20°. Performance plateaus at a spatial frequency of ~6.4 c.p.d, and in all subsequent experiments we employ elements with spatial frequencies in the range indicated. Squares show path-detection performance, as a function of carrier spatial frequency, when half of the elements are removed. Both subjects are at chance, thus indicating that performance in subsequent experiments, with paths composed of alternating carrier frequency, cannot be attributable to the detection of contour structure in a single population.

Notice that performance plateaus within the range of carrier spatial frequencies bracketed in Fig. 3; for a given spatial frequency there is a wide range of separations that produce near-optimal contour-detection performance. The spacing of elements in the two highest-frequency conditions falls outside of that range. The presence of a plateau also means that there is relatively little effect of decreasing the spatial frequency of the carrier over a two-octave range, even though this increases the orientational bandwidth of elements considerably. It appears that as long as the element delivers an orientation signal, our confidence in this signal has little influence on contour detectability. This is consistent with the finding that jittering element contrast has little effect on contour integration[19] and, more generally, with observers' insensitivity to the spatial frequency of gratings in orientation judgments.[33]

These data suggest that, for a given set of stimulus parameters, it is possible to isolate a range of element spatial frequencies that lead to broadly similar levels of contour detectability. In all subsequent experiments reported the spatial frequencies of the two intermixed populations of elements were drawn from within the bracketed range shown in Fig. 3.

The second part of this experiment was a control condition for subsequent conditions and tested the performance of subjects when the contrast of half of the elements in the texture was randomly set to zero. For the element density tested, both subjects' performance (squares in Fig. 3) falls consistently to chance. This indicates that if observers were to simply ignore the presence of one set in any of the following conditions, they would be unable to perform the task.

## 4. EXPERIMENT 2: TOLERANCE TO VARIATION IN SPATIAL FREQUENCY WITHIN A CONTOUR

Experiment 2 examined the spatial-frequency tuning of the contour-extraction mechanism by use of embedded paths composed of elements whose spatial frequency alternates between two values along the contour. The technique of varying stimulus attributes across alternating path elements has been successfully employed elsewhere to investigate integration across color,[31] and depth.[9]

### A. Stimuli

The Gabor patches that compose the path stimuli for this experiment were drawn from two populations with a varying degree of similarity between their spatial frequencies. Having established the range of spatial frequencies that produce a constant level of performance, we restricted the frequency of elements to that range. One set of elements was always assigned a spatial frequency of 3.2 c.p.d. (the value falling in the center of the permissible range) and the other set was assigned a spatial frequency of between 1.6 and 6.4 c.p.d., sampled in quarter-octave steps. Figure 4 shows examples of the stimuli used.

To examine how varying the path angle interacts with spatial-frequency tuning, we wished to avoid the known advantage for detecting straighter paths; i.e., we wanted to equalize performance across all path angles for contours composed of elements of the same spatial frequency. This was to avoid both ceiling effects for straight paths (near-perfect performance for 0° and 10° path angles) and floor effects for curved paths that might mask any effects of spatial-frequency alternation per se. We performed a series of pilot experiments to determine which stimulus parameter might be altered to best match baseline performance (i.e., matched spatial frequency of the two populations) across path angle. Having tested the effects of positional and orientational jitter imposed on elements, as well as various spacing parameters, we converged on path length as the parameter used to equalize performance across path angle. We chose path length because its alteration results only in a larger sample of the path being

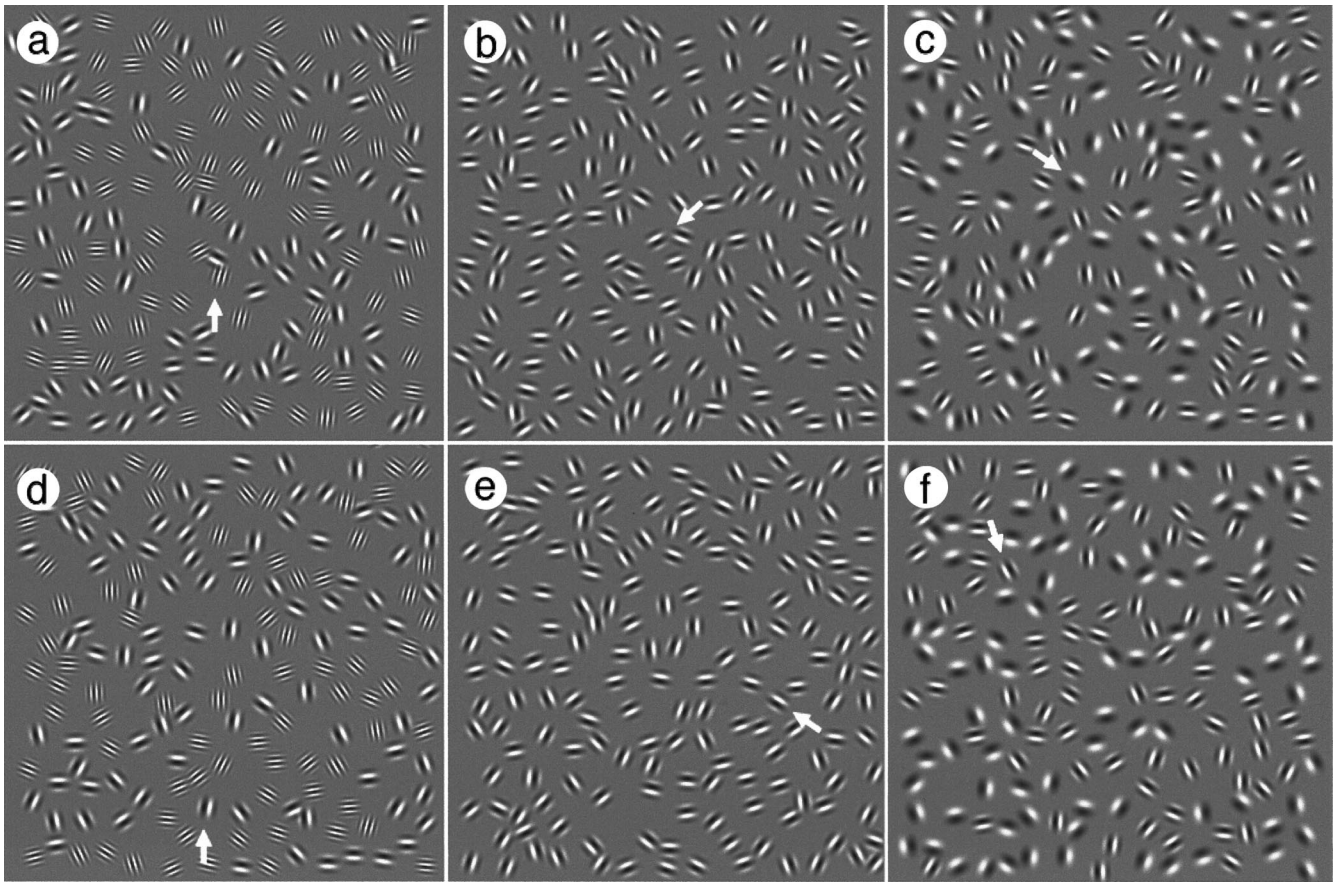


Fig. 4. Examples of the stimuli from experiment 2. (a)–(c) 4-element path with a path angle of 0°, (d)–(f) 8-element path with a path angle of 20°. For all textures the spatial frequency of one set is 3.2 c.p.d. and of the second set [(a),(d)] 6.4 (b),(e) 3.2, and [(c),(f)] 1.6 c.p.d. Note that the effect of mixing the frequency of elements is more disruptive to the detection of curved paths in (d) and (f) than straight paths in (a) and (c). Arrows indicate the first element of all paths.

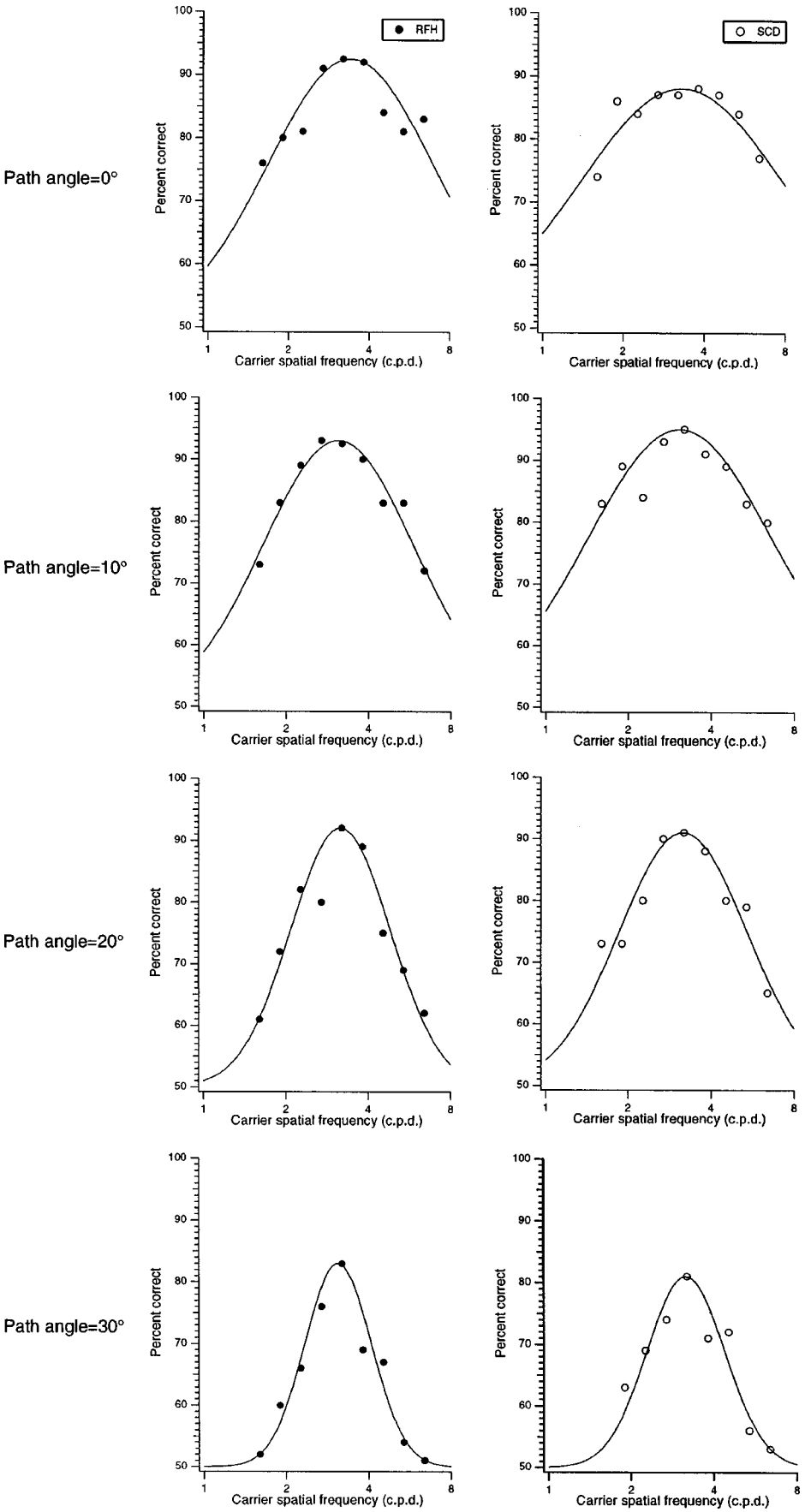


Fig. 5. Tuning of contour detection for the spatial frequency of contour components at different path angles. Data from two subjects are shown. Notice the sharpening of tuning with increasing path angle.

presented to subjects (the local statistics of element position and orientation are maintained across conditions). We found path lengths of 4 (path angle of 0°), 6 (path angle of 10°), 8 (path angle of 20°), and 10 (path angle of 30°) matched performance of both subjects at ~85%–90%. This level of performance is clearly below ceiling but allows for reliable detection of deterioration in performance across the conditions tested.

### B. Results

Figure 5 shows results from this experiment. The graphs in the top part of the figure demonstrate that subjects' detection of straight paths does not drop below 74% in the presence of maximum frequency variation (one octave) within the contour. Given the spatial-frequency tuning of cortical mechanisms (typically ~1 octave)[34–39] the preprocessing stages of all models described in Section 1 should fail to group contour elements. It would be straightforward to generalize the iterative, postfiltering class of model to receive input from multiple scales. This result is more problematic for the feed-forward approaches, which modify mechanisms at the point of filtering, and Gigus and Malik,[20] for example, acknowledge that lack of scale-invariant grouping is a potential weakness of this class of model.

Data in Fig. 5 were fit (solid curves) with Gaussians defined as

$$G(x) = A + B \exp\left\{-\left[\frac{\mu - \log(x)}{\sigma}\right]^2\right\}, \qquad (3)$$

where

$$A = 50, \qquad B = pc_{\max}.$$

Here $pc_{\max}$ is the maximum performance for that condition. This function produces fits that are symmetrical on a log $x$ axis, fall to 50% performance, and peak at the

**Table 1. Half-Width at Half-Height of the Tuning Functions Shown in Fig. 5**[a]

| Path Angle | RFH | SCD |
|---|---|---|
| 0° | 1.15 | 1.43 |
| 10° | 1.06 | 1.23 |
| 20° | 0.82 | 0.94 |
| 30° | 0.69 | 0.73 |

[a] Values given are octaves of spatial scale.

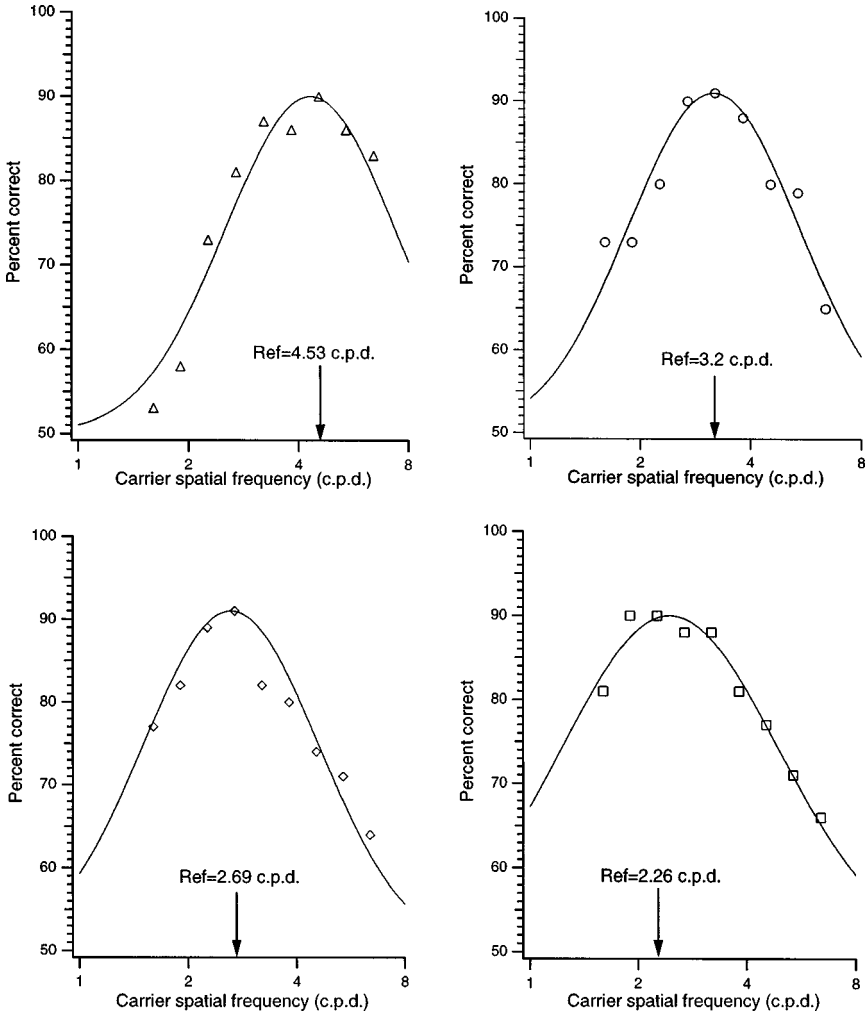


Fig. 6. Spatial-frequency tuning for detection of contours (path angle of 20°; subject SCD) for four referent spatial frequencies. Peak performance and width of tuning curves are similar across all referent frequencies.

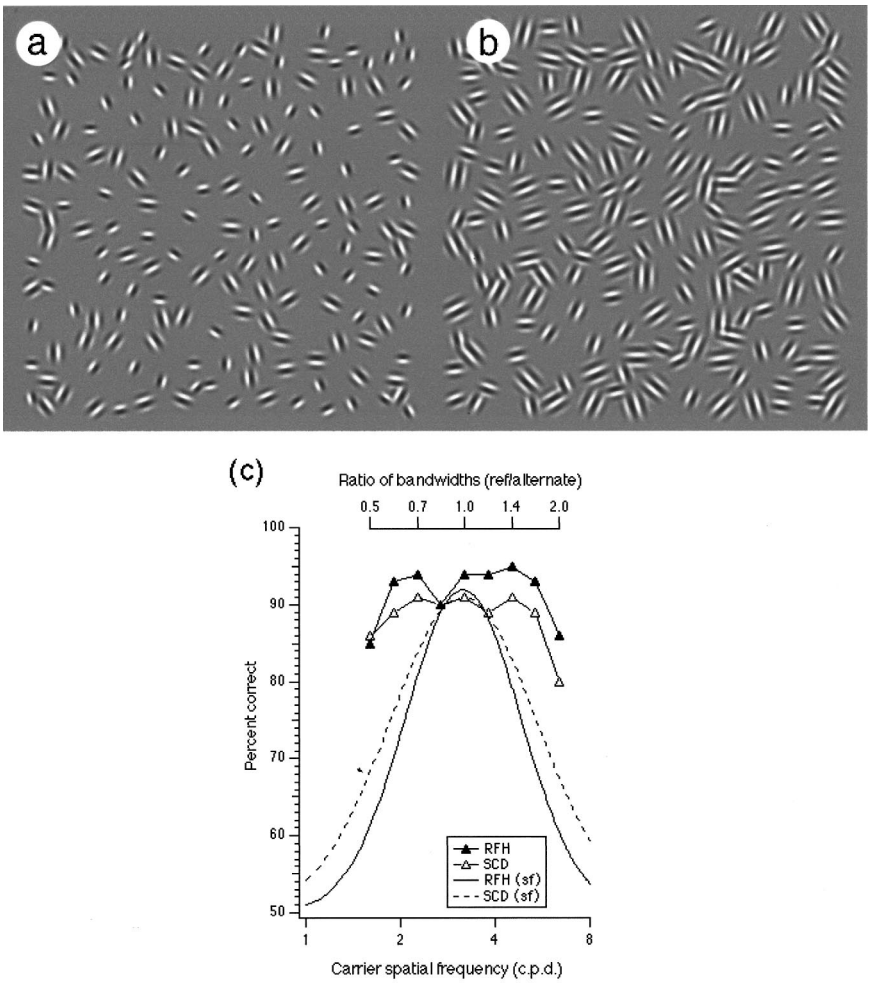


Fig. 7. (a),(b) Stimuli from the control condition assessing the effect of bandwidth alternation in the absence of spatial-frequency change. The paths shown (20° path angle) are composed of reference patches alternating with micropatterns with envelope standard deviations equal to (a) 0.71 and (b) 1.41 times that of the reference envelope. (c) Results (triangles, upper abscissa) indicate only a small reduction of performance with bandwidth alternation compared with the equivalent spatial-frequency alternation condition (solid and dashed curves).

maximum level of performance for that condition. The half-width at half-height values for these fits are shown in Table 1.

Notice that there is a consistent increase in the spatial-frequency tuning of contour extraction as the curvature of the contour increases. This is an unexpected result. If a common mechanism underlies detection of all contours, one might expect spatial frequency tuning to remain constant. Is this result entirely due to the requirements of the task, or does it accurately reflect the operation of the mechanisms underlying all contour detection?

All the data described were measured for a single reference spatial frequency, falling in the center of the permissible range estimated in experiment 1 (3.2 c.p.d.). To ensure that tuning does not depend critically on the choice of referent frequency, we conducted a control experiment, measuring the tuning for detection of contours with a path angle of 20° at three other referent frequencies half an octave above and a quarter- and a half-octave below the standard referent (corresponding to spatial frequencies of 4.53, 2.69, and 2.26 c.p.d., respectively). Graphed data from this condition are shown in Fig. 6 (as well as the data collected with 20° paths with the default referent spatial frequency). Note that all tuning curves peak around the referent wavelength and that width of tuning is similar for the three extra referent frequencies tested. Half-height at half-widths are 0.97 octaves (ref = 4.53 c.p.d.), 0.94 octaves (ref = 3.2 c.p.d.), 1.07 octaves (ref = 2.69 c.p.d.), and 1.12 octaves (ref = 2.26 c.p.d.). While there is a small increase in bandwidth for decreasing referent spatial frequency, all bandwidths are narrower than bandwidths for 10° path angles (mean of 1.23 octaves).

It was noted in Section 2 that by using the same size envelope but alternating the spatial frequency of micropatterns, one is also changing their spatial and orientational bandwidths. We conducted a further control experiment to determine the degree to which the tuning observed could be attributable to changes in local bandwidth. Paths with a 20° path angle were composed of alternate reference patches (carrier at 3.2 c.p.d., envelope with a standard deviation of 9.4 arc min) and patches with the same carrier wavelength but with different envelope sizes. We tested envelope standard deviations of between 4.7 arc min and 18.8 arc min in quarter-octave steps. This produces changes in bandwidth along the

contour that correspond exactly to the changes brought about in the spatial-frequency alternation condition described (the nonreference patches can actually be thought of as being similar to those used in the spatial-frequency condition but locally scaled to have the same wavelength as the referent).

Unfortunately, changing the patch size produces side effects. Although carrier wavelength is thought to be the major determinant of whether the spacing of a path stimulus leads to grouping, this, as stated above, may be an oversimplification. When the envelope is very small, micropatterns appear more sparsely distributed [Fig. 7(a)], and a reduction in performance might be expected. Increasing envelope size leads to the opposite problem: extremely dense [Fig. 7(b)] textures that might also baffle the contour-extraction system. Results from this condition are shown in Fig. 7(c) and compared with the equivalent spatial-frequency alternation condition for both subjects. Bandwidth actually has little effect on performance until the test micropatterns' envelopes are approximately double the size of the referents' when we see a reduction of ~10% in performance (compared with ~25% for the spatial-frequency condition). Subjectively this is due to the extremely dense and confusing nature of stimuli in this condition and not to a failure to group along the contour. We conclude from this condition that micropattern bandwidth is unlikely to have contributed significantly to the main results reported for experiment 2.

Our data do not exclude the possibility that changes in tuning arise because detection of straight paths might not require explicit filter linking at all. We showed previously that detection of near-straight contours can be modeled successfully with the output of multiple, independent, coarse-scale oriented filters and that such a system can explain contour linking in the periphery.[32] The observed reduction in tuning could be due to a switch from the use of this type of coarse filtering operating at one orientation, which will have broad tuning for the spatial frequency of contour elements, to a mechanism operating across orientation that links the output of a series of more narrowly tuned detectors. We know that linking of straight paths in foveal vision is not subserved exclusively by such a mechanism; if that were the case, we would be unable to see contours composed of phase-reversing Gabor elements in fovea, which we can with only a moderate reduction in performance.[40] To test whether narrower tuning could be attributed to the operation of independent oriented filters, we measured tuning for straight (0° path angle) and curved (30° path angle) contours composed of elements in which the carrier phase of adjacent elements differed by 180°. We ob-

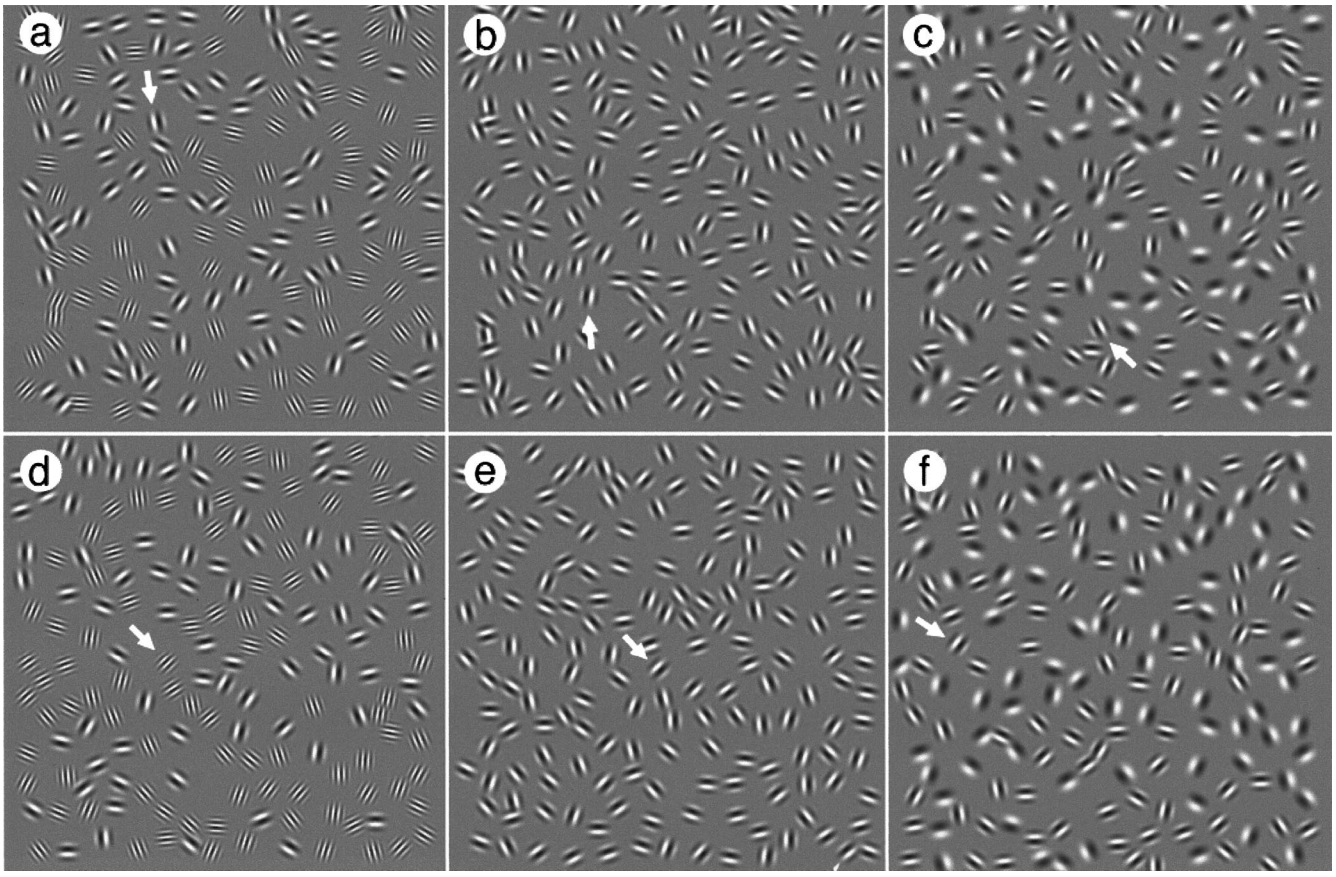


Fig. 8. Examples of the stimuli from experiment 3. (a)–(c) Smooth paths with a path angle of 20°, (d)–(f) closed paths of 12 elements with 30° path angle. Elements in (b) and (e) are of a single spatial frequency, but one population in (a) and (d) and (c) and (f) is made up of elements with a peak spatial frequency one octave higher or lower, respectively. Arrows indicate position and orientation of the first path element.

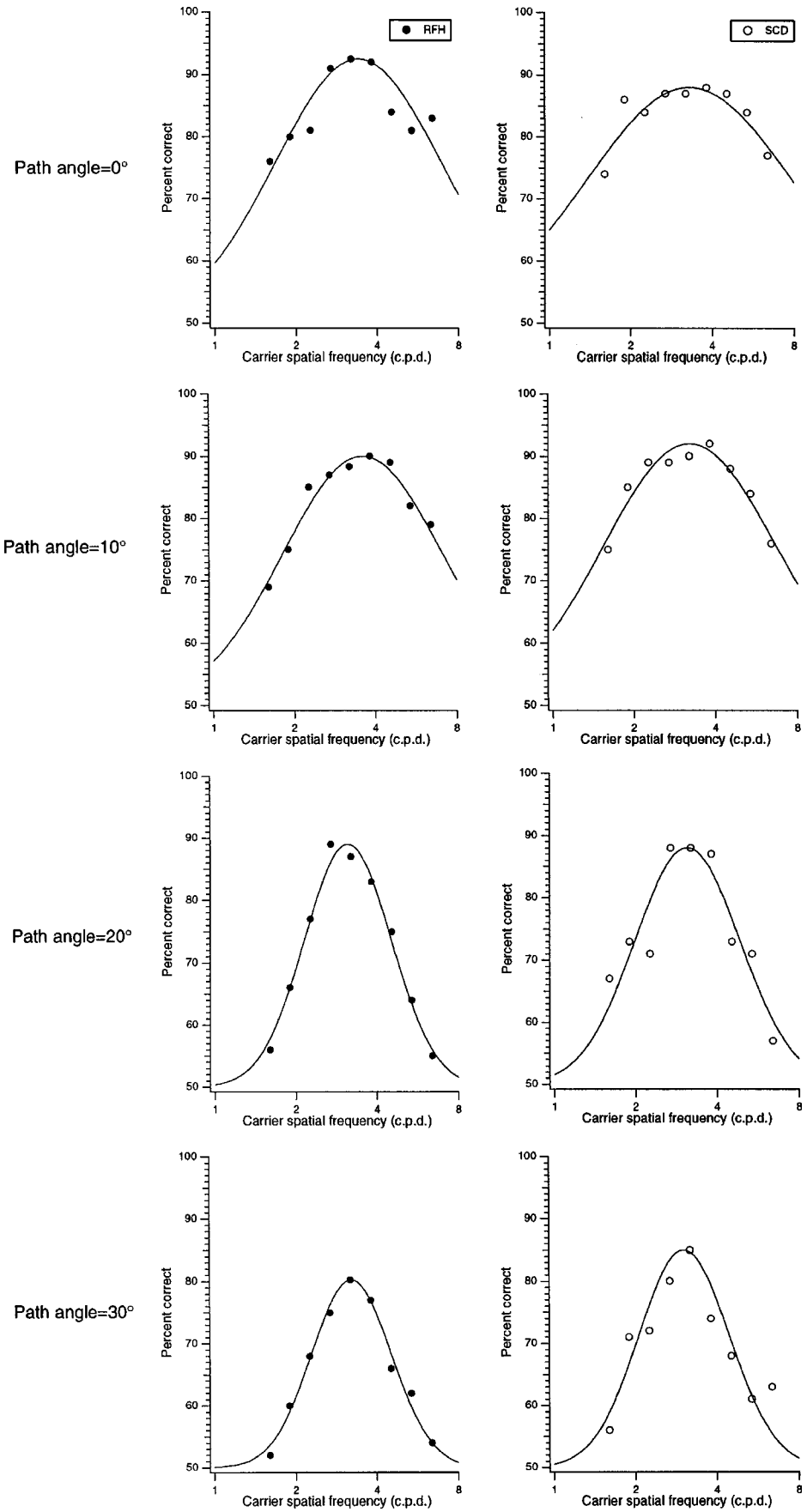


Fig. 9. Spatial-frequency tuning for smooth contours (uppermost graphs are taken from the straight path condition of Fig. 4). Tuning functions are similar to those for jagged contours.

served no substantial difference in tuning compared with the phase-matched condition. We conclude that observed changes in spatial tuning are not due to the operation of a different mechanism for grouping straight paths but instead are an inherent property of the general intercellular linking process that subserves contour integration.

We next consider the possibility that it is the jagged nature of the contours employed that forces subjects, at large path angles, into using a narrow range of filters to pair-wise group elements along the path. In experiment 3 we addressed this possibility by measuring spatial-frequency tuning for detection of contours containing only smooth orientation change.

## 5. EXPERIMENT 3: RESISTANCE TO SPATIAL-FREQUENCY VARIATION IN SMOOTH AND CLOSED CONTOURS

The findings reported for general contour detection[1] have been confirmed for smooth contours[41] for which adjacent path elements always have orientation differences in the same direction [e.g., Fig. 8(b)]. Contours containing smoothly changing orientations are easier to detect,[41] as are closed contours[2,3] (although the latter finding is closely related to the former because the introduction of an orientation discontinuity into an otherwise smooth closed contour reduces detectability drastically).[41] The procedure used for the experiments reported thus far is to randomly assign the direction of orientation change between adjacent contour elements. We wished to test whether spatial-frequency tuning for smooth contours might be different from tuning for these jagged contours or whether the tuning observed was a general property of contour integration. To this end we repeated the procedure described for experiment 2 for paths with smooth orientation changes. In addition, we examined path lengths that, in conjunction with a smooth orientation change, would lead to path closure.

### A. Stimuli

Stimuli were generated as described in Subsection 4.A except that, within a stimulus, orientation changes between successive elements were constrained to be either consistently clockwise or counterclockwise. This produces contours with smoothly changing orientations. Closed contours were simply smooth paths composed of 12 elements that have a 30° orientation difference between successive elements. Typical examples of both types of stimulus are shown in Fig. 8.

### B. Results

Results, which are plotted in Fig. 9, prove to be very similar to those obtained with jagged contours. Table 2 tabulates the half-width at half-height of spatial-frequency tuning. The same sharpening of tuning is observed with increasing path angle. Table 2 also gives the improvement, in percentage points, for the matched spatial-frequency condition with smooth compared with jagged paths. There is little or no consistent improvement at small path angles. This is consistent with previous findings that demonstrate that any advantage for smooth versus jagged contours are small and arise only at large path angles[41] (30° or greater).

**Table 2. Half-Width at Half-Height Measures Derived from the Tuning Functions Shown in Fig. 9[a]**

| Path Angle (Smooth) | RFH | Improvement (%) | SCD | Improvement (%) |
|---|---|---|---|---|
| 0° | 1.15 | — | 1.43 | — |
| 10° | 1.15 | −4.2 | 1.23 | −8 |
| 20° | 0.78 | −5.3 | 0.85 | −4 |
| 30° | 0.74 | −2.5 | 0.79 | +4.0 |
| 30° (closed) | 0.75 | +5.0 | 0.78 | +9.0 |

[a] Values given are in octaves of spatial scale. Also shown are the difference in peak performance (i.e., for matched spatial-frequency populations) between smooth and jagged path conditions.

A comparison of tuning for closed versus open contours is made in Fig. 10, showing only a slight advantage for closed contours. However, this could be attributable to the greater length (12 versus 10 elements). The same tuning function, derived from the open 30° path-angle data and displaced vertically, provides a good fit to data from both the closed and the open contour conditions. In summary, since there is no evidence to suggest that spatial-frequency tuning for open and closed paths differs substantially or that performance with smooth and jagged paths differs substantially, we interpret the spatial-frequency tuning observed as a general property of the contour-integration system.

## 6. GENERAL DISCUSSION

We have demonstrated that the visual contour-integration system is tuned for the spatial-frequency content of the contour and specifically narrows with increasing contour curvature. This is attributable neither to the operation of low-frequency grouping operation for near-straight paths nor to the jagged nature of element-orientation change within the contour but seems to be a property of a general integration mechanism. What implications does this have for existing computational models of contour integration?

That Gabor spatial frequency affects performance at all indicates that the contour-extraction process does not simply extract the local orientation of elements of band-pass path stimuli and operate on some abstracted orientation field [i.e., the model shown in Fig. 1(a) is incorrect]. This is problematic for both iterative postfiltering and feed-forward systems operating within a single spatial band on filter kernels at a single bandwidth. Our data suggest that to accommodate these findings, postfiltering consistency measures must either have simultaneous access to filter outputs at all scales and weight contributions of different frequencies according to local contour curvature or address the problem of integrating the output of detectors at various bandwidths into a single representation. Results are also inconsistent with pure feed-forward mechanisms that locally modify the operation of filters. Within this framework, our data suggest

that the spatial bandwidth of filtering mechanisms differs for integration at different curvatures. This type of general scheme would, however, be consistent with neurophysiological data that suggest spatial bandwidths of oriented cells in V1 vary considerably in cats[35,37–39] and monkeys.[34,36]

An alternative interpretation of the change in tuning that we observed is that the contour-detection system may be exploiting the greater interscale support that straight edges enjoy.

Figure 11 shows four step edges of increasing curvature. Below each is a histogram of the response (at the position indicated by the arrow) of a bank of Gabor filters[42] extending over three octaves of scale (high to low spatial frequencies from left to right). For near-straight edges, the histogram is approximately flat, thus indicating similar responses from filters across scale and a high degree of interscale support. As curvature increases, the contour increasingly favors the high spatial frequencies, and scale support decreases. This is a simple consequence of the fact that oriented filters signal the degree of local colinearity of image structure at the scale of the filter employed. Thus the linking process for straight edges need not be as precisely tuned for local spatial-frequency content as the curved-edge linking process because the presence of a straight contour is supported by the activity of filters at a range of scales. Integrating over the maximum range of filters is desirable for a number of reasons, not the least of which is overcoming the effects of noise (which will tend to be uncorrelated across scale[43]). Given that much orientation structure in natural images arises from the presence of edges,[21] the narrowing of filter responses with contour curvature could be attributable to a rigid-scale combination component of the contour linking process that is designed to operate on phase-congruent curvilinear image structure (such as edges). Phase congruence could be registered by means of the operation of edge-detecting receptive fields or by an

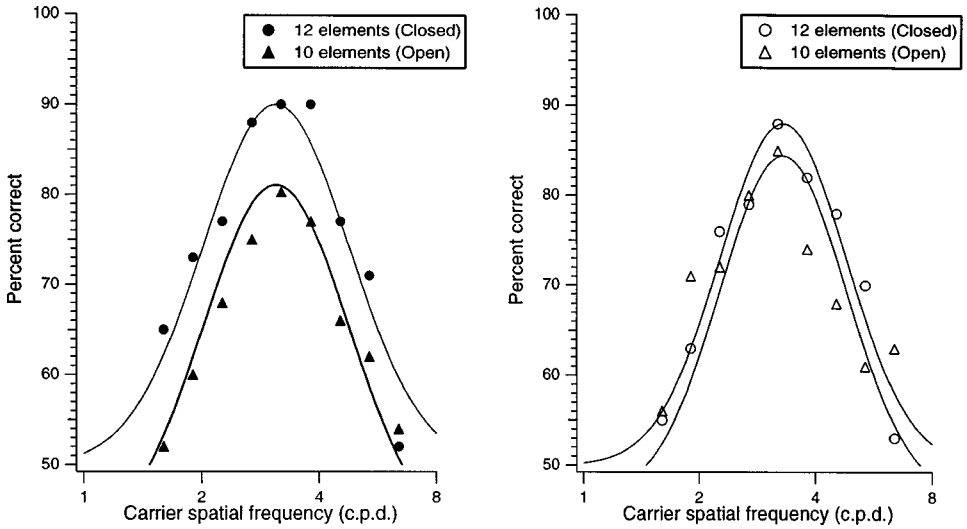


Fig. 10. Two subjects' spatial-frequency tuning for closed versus open contours. Performance with a smooth contour and the same path angle is also shown (triangles). The two sets of data are fitted with the same tuning curve, with a constant offset subtracted for the smooth path data. Similar tuning is obtained.

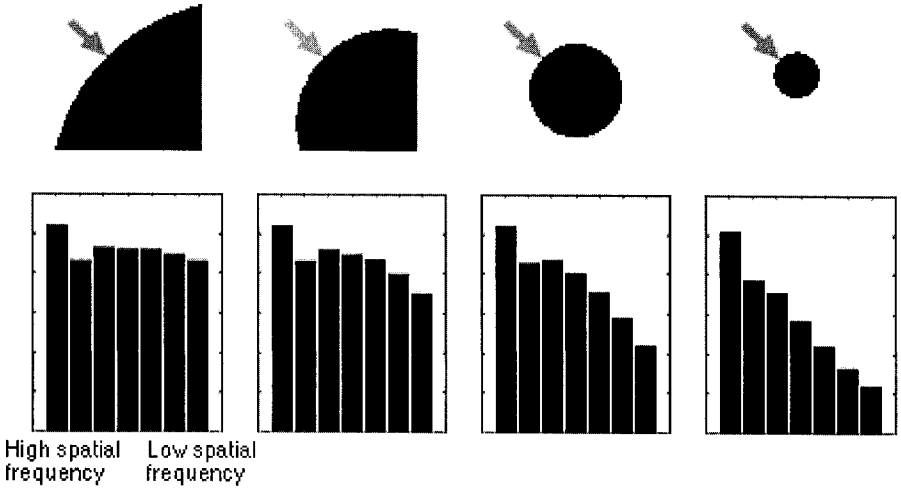


Fig. 11. The degree of scale support provided by edges as a function of their curvature. Edge curvature increases, from left to right in the figure. Histograms show the response of weighted Gabor filters, at the position marked by the arrows, across three octaves of scale (fine to coarse from left to right). Support is consistent across scale for near-straight edges (leftmost histogram) but drops away sharply for increasingly curved edges.

explicit, interscale combination system. With respect to the former approach, it has been observed that unsupervised learning of sparse image codes produces oriented receptive fields at a range of bandwidths,[44] including edge filters.[45] Functionally, edge filters could be useful for coding straight edges, while filters of increasingly narrow bandwidth would be suitable for capturing curved-edge structures. The alternative approach, employing explicit and rigid linking between spatial scales, is embodied in systems such as MIRAGE.[43] It remains to be seen whether the contour-integration paradigm can offer insights into the role and nature of scale-linking operations that underlie the visual processing of two-dimensional form.

## ACKNOWLEDGMENTS

Thanks to Stephane Rainville, Tim Meese, and Isabelle Mareschal for valuable suggestions relating to this project. This work was funded by grant MT 108-18 from the Canadian Medical Research Council to R. F. Hess.

S. C. Dakin's e-mail address is scdakin@vision.mcgill.ca.

## REFERENCES AND NOTES

1. D. J. Field, A. Hayes, and R. F. Hess, "Contour integration by the human visual system: evidence for a local 'association field,' " Vision Res. **33**, 173–193 (1993).
2. I. Kovacs and B. Julesz, "A closed curve is much more than an incomplete one: effect of closure in figure-ground segmentation," Proc. Natl. Acad. Sci. USA **90**, 7495–7497 (1993).
3. I. Kovacs and B. Julesz, "Perceptual sensitivity maps within globally defined visual shapes," Nature **370**, 644–646 (1994).
4. J. T. Smits and P. G. Vos, "The perception of continuous curves in dot stimuli," Perception **16**, 121–131 (1987).
5. Z. Pizlo, M. Salach-Golyska, and A. Rosenfeld, "Curve detection in a noisy image," Vision Res. **37**, 1217–1241 (1997).
6. L. Glass, "Moiré effects from random dots," Nature **243**, 578–580 (1969).
7. T. Caelli and B. Julesz, "Psychophysical evidence for global feature processing in visual texture discrimination," J. Opt. Soc. Am. **69**, 675–678 (1979).
8. S. C. Dakin, "The detection of structure in Glass patterns: psychophysics and computational models," Vision Res. **37**, 2227–2259 (1997).
9. R. F. Hess and D. J. Field, "Contour integration across depth," Vision Res. **35**, 1699–1711 (1995).
10. S. W. Zucker, "Early orientation selection: tangent fields and the dimensionality of their support," Comput. Vis. Graph. Image Process. **8**, 71–77 (1985).
11. S. W. Zucker, C. David, A. Dobbins, and L. Iverson, "The organization of curve detection: coarse tangent fields and fine spline coverings," in *Proceedings of the IEEE International Conference on Computer Vision* (IEEE Computer Society Press, Los Alamitos, Calif., 1988).
12. P. Parent and S. W. Zucker, "Trace inference, curvature consistency and curve-detection," IEEE Trans. Pattern. Anal. Mach. Intell. **11**, 823–839 (1989).
13. S. W. Zucker, A. Dobbins, and L. Iverson, "Two stages of curve detection suggest two styles of visual computation," Neural Computation **1**, 68–81 (1989).
14. A. Sha'ashua and S. Ullman, "Structural saliency: the detection of globally salient structures using a locally connected network," in *Proceedings of the IEEE International Conference on Computer Vision* (IEEE Computer Society Press, Los Alamitos, Calif., 1988), pp. 321–327.
15. S.-C. Yen and L. H. Finkel, "Salient contour extraction by temporal binding in a cortically based network," in *Advances in Neural Information Processing Systems*, D. S. Touretzky, M. C. Mozer, and M. E. Hasselmo, eds. (MIT Press, Cambridge, Mass., 1996).
16. S.-C. Yen and L. H. Finkel, "Cortical synchronization mechanism for 'pop-out' of salient image contours," in *The Neurobiology of Computation*, J. Bower, ed. (Kluwer Academic, Boston, Mass., 1996).
17. W. H. Freeman and E. H. Adelson, "The design and use of steerable filters," IEEE Trans. Pattern. Anal. Mach. Intell. **13**, 891–906 (1991).
18. U. Polat and D. Sagi, "The architecture of perceptual spatial interactions," Vision Res. **34**, 73–78 (1994).
19. R. F. Hess, S. C. Dakin, and D. J. Field, "The role of 'contrast enhancement' in the detection and appearance of visual contours," Vision Res. **38**, 783–787 (1998).
20. Z. Gigus and J. Malik, "Detecting curvilinear structure in images," Department of Computer Science Tech. Rep. 96/619 (University of California Berkeley, Berkeley, Calif., 1991).
21. D. J. Field, "Scale-invariance and self-similar 'wavelet' transforms: an analysis of natural scenes and mammalian visual systems," in *Wavelets, Fractals and Fourier Transforms*, M. Marge, J. C. R. Hunt, and J. C. Vassilicos, eds. (Clarendon, Oxford, UK, 1993), pp. 151–193.
22. D. Marr and E. Hildreth, "Theory of edge detection," Proc. R. Soc. London Ser. B **207**, 187–217 (1980).
23. D. Marr, *Vision* (Freeman, San Francisco, Calif., 1982).
24. J. F. Canny, "Finding edges and lines in images," MIT Artificial Intelligence Laboratory Tech. Rep. 720 (Massachusetts Institute of Technology, Boston, Mass., 1983).
25. D. G. Lowe, "Organization of smooth image curves at multiple spatial scales," in *Proceedings of the IEEE International Conference on Computer Vision* (IEEE Computer Society Press, Los Alamitos, Calif., 1988), pp. 119–130.
26. A. Hayes, "Representation by images restricted in resolution and intensity range," Ph.D. dissertation (University of Western Australia, Perth, Australia 1989).
27. L. D. Harmon and B. Julesz, "Masking in visual recognition: effects of two dimensional filtered noise," Science **180**, 1194–1197 (1973).
28. M. C. Morrone and D. C. Burr, "Capture and transparency in coarse quantized images," Vision Res. **37**, 2609–2629 (1997).
29. S. J. M. Rainville, F. A. A. Kingdom, and A. Hayes, "Is motion perception sensitive to local phase structures?" Invest. Ophthalmol. Visual Sci. **38**, S215 (1997).
30. D. G. Pelli, "The VideoToolbox software for visual psychophysics: transforming number into movies," Spatial Vis. **10**, 437–442 (1997).
31. W. H. McIlhagga and K. T. Mullen, "Contour integration with colour and luminance contrast," Vision Res. **36**, 1265–1279 (1996).
32. R. F. Hess and S. C. Dakin, "Absence of contour linking in peripheral vision," Nature **390**, 602–604 (1997).
33. D. W. Heeley and H. M. Buchanan-Smith, "Recognition of stimulus orientation," Vision Res. **32**, 719–743 (1990).
34. P. H. Schiller, B. L. Finlay, and S. F. Volman, "Quantitative studies of single-cell properties in monkey striate cortex: III. Spatial frequency, J. Neurophysiol. **39**, 1334–1351 (1976).
35. J. Movshon, I. D. Thompson, and D. J. Tolhurst, "Spatial and temporal contrast sensitivity of neurones in area 17 and 18 of the cat's visual cortex," J. Physiol. (London) **283**, 101–120 (1978).
36. J. J. Kulikowski and P. O. Bishop, "Linear analysis of the responses of simple cells in the cat visual cortex," Exp. Brain Res. **44**, 386–400 (1981).
37. D. J. Tolhurst and I. D. Thompson, "On the variety of spatial frequency selectivities shown by neurons in area 17 of the cat," Proc. R. Soc. London Ser. B **213**, 183–199 (1981).
38. R. L. De Valois, D. G. Albrecht, and L. G. Thorell, "Spatial frequency selectivity of cells in macaque visual cortex," Vision Res. **22**, 545–559 (1982).
39. D. J. Field and D. J. Tolhurst, "The structure and symme-

try of simple-cell receptive-field profiles in the cat's visual cortex," Proc. R. Soc. London Ser. B **228**, 379–400 (1986).
40. D. J. Field, A. Hayes, and R. F. Hess, "The role of phase and contrast polarity in contour integration," Invest. Ophthalmol. Visual Sci. **38**, S999 (1997).
41. M. W. Pettet, S. P. McKee, and N. M. Grzywacz, "Smoothness constrains long-range interactions mediating contour-detection," Invest. Ophthalmol. Visual Sci. **37**, 4368 (1996).
42. Gabor filters had 1:1 envelopes, with a wavelength equal to $1.5\sigma$, and were in cosine phase. Their outputs were weighted by $1/f$.
43. R. J. Watt and M. J. Morgan, "A theory of the primitive spatial code in human vision," Vision Res. **25**, 1661–1674 (1985).
44. B. A. Olshausen and D. J. Field, "Emergence of simple-cell receptive field properties by learning a sparse code for naturla images," Nature **381**, 607–609 (1996).
45. A. J. Bell and T. J. Sejnowski, "The 'independent components' of natural scenes are edge filters," Vision Res. **37**, 3327–3338 (1997).